Efficient Catalysis of Hydrogen Evolution Reaction from $WS_{2(1-x)}P_{2x}$ Nanoribbons

*Tofik Ahmed Shifa, Fengmei Wang, Kaili Liu, Zhongzhou Cheng, Kai Xu, Zhenxing Wang, Xueying Zhan, Chao Jiang, and Jun He**

***T**he rational design of Earth abundant electrocatalysts for efficiently catalyzing hydrogen evolution reaction (HER) is believed to lead to the generation of carbon neutral energy carrier. Owing to their fascinating chemical and physical properties, transition metal dichalcogenides (TMDs) are widely studied for this purpose. Of particular note is that doping by foreign atom can bring the advent of electronic perturbation, which affects the intrinsic catalytic property. Hence, through doping, the catalytic activity of such materials could be boosted. A rational synthesis approach that enables phosphorous atom to be doped into WS_2 without inducing phase impurity to form $WS_{2(1-x)}P_{2x}$ nanoribbon (NRs) is herein reported. It is found that the $WS_{2(1-x)}P_{2x}$ NRs exhibit considerably enhanced HER performance, requiring only −98 mV versus reversible hydrogen electrode to achieve a current density of −10 mA cm^{-2}. Such a high performance can be attributed to the ease of H-atom adsorption and desorption due to intrinsically tuned WS_2, and partial formation of NRs, a morphology wherein the exposure of active edges is more pronounced. This finding can provide a fertile ground for subsequent works aiming at tuning intrinsic catalytic activity of TMDs.*

T. A. Shifa, F. M. Wang, K. Liu, Z. Z. Cheng, K. Xu, Dr. Z. Wang, X. Zhan, Prof. J. He
CAS Center for Excellence in Nanoscience
CAS Key Laboratory of Nanosystem and Hierarchical Fabrication
National Center for Nanoscience and Technology
Beijing 100190, China
E-mail: hej@nanoctr.cn

T. A. Shifa, F. M. Wang, K. Liu, K. Xu
University of Chinese Academy of Sciences
Beijing 100049, China

Z. Z. Cheng
University of Science and Technology Beijing (USTB)
No.30, Xueyuan Road, Haidian District, Beijing 100083, China

Prof. C. Jiang
CAS Key Laboratory of Standardization and Measurement for Nanotechnology
National Center for Nanoscience and Technology
Beijing 100190, China

DOI: 10.1002/smll.201603706

1. Introduction

Nowadays, the world is more focused on responding to the ever-increasing energy demand without compromising environmental benignity. The abundantly used fossil fuel has a serious environmental problem, which leads the globe to the undesired future.[1–3] In an effort of sustainably powering the globe, electrocatalytic hydrogen production takes significant concern of the scientific community.[4,5] However, this route has to be catalyzed by rarely available and expensive noble metals, such as Pt and Pd, which impede the scalability.[6,7] Thus, it is highly essential to explore Earth abundant electrocatalysts for realization of the anticipated green energy future. Considerable progress has been made in such research endeavors that communicated variety of materials, including nitrides, carbides, chalcogenides, phosphides, etc.[8–12] In particular, transition metal dichalcogenides (TMDs) have attracted growing interest since the breakthrough report by Jaramillo et al.,[13] demonstrating the fact

that the edge of MoS_2 is active for the catalysis of hydrogen evolution reaction. Of particular note is that the low Gibbs free energy, as theoretically calculated,[14] of hydrogen adsorption on the edge of WS_2 initiated intense investigations based on this material.[15–17] To further improve the intrinsic catalytic activity, the design of ternary structure plays a pivotal role via tailoring the inherent electronic structure. For instance, Q. Gong et al.[18] showed the improved performance of $MoS_{2(1-x)}Se_{2x}$ nanoflakes as compared to the corresponding binary ones. Our group has also demonstrated the significantly enhanced performance of $WS_{2(1-x)}Se_{2x}$ nanotubes[19] and nanoribbons (NRs).[20] Many others have also been fabricated in pursuit of enhanced activity.[21–26] Formation of ternary nanomaterials is believed to bring the hydrogen adsorption free energy closer to a thermoneutral value, which is fertile ground for hydrogen evolution reaction (HER). More impressively, it would result in the most pragmatic means of tuning the electronic environment when an atom from different group is doped without any discernible phase impurity as exhibited by CoPS.[27–29] These materials perform by far better than those of CoSSe.[30,31] Doping of low electronegative phosphorous atom gives rise to the electronic perturbation that would ultimately engineer the intrinsic property of the host material toward a favorable condition for hydrogen atom to be adsorbed and desorbed.[28,32] However, this attempt is limited in pyrite phase structured TMDs and little attention is, so far, paid for the layered types.

Herein, we demonstrate the synthesis of $WS_{2(1-x)}P_{2x}$ NRs via hydrothermal method, for WO_3 nanowires (NWs) formation, followed by simultaneous sulfurization and phosphorization reaction. In the later operation, the neighboring NWs of WO_3 got interconnected with each other due to the simultaneous action, which resulted in doped NR. This method brought the advent of tuning the morphology from NW to NR that provides geometrically exposed catalytic sites. Significantly, the electronic perturbation occurred in WS_2 after introducing P atoms. Benefiting from these advantages, the doped NR demonstrates a very good catalytic activity in HER as evidenced from the recorded low overpotential of –98 mV (vs reversible hydrogen electrode (RHE)) at –10 mA cm^{-2} and small Tafel slope of 71 mV per decade, remarkably outperforming that of pure WS_2. This study demonstrates the first report in incorporating P into layered WS_2 that would enable it to represent a very promising approach of designing electrocatalysts with improved HER catalytic activity.

2. Results and Discussion

The experimental setup of our synthesis detail is schematically illustrated in **Figure 1**a. As can be seen, the $WS_{2(1-x)}P_{2x}$ NR was obtained via a two-step method comprising hydrothermal and chemical vapor deposition. In the first step, densely grown WO_3 NWs were obtained on carbon fiber (CF) substrate. All the fibers are fully covered by WO_3 NWs (Figure S1, Supporting Information). This hydrothermally grown WO_3 NWs/CF was then placed at the back zone of chemical vapor deposition (CVD) tube wherein the front zone was loaded with mixed powders of P and S (see the Experimental Section and Figure S2, Supporting Information) for simultaneous phosphidation and sulfidation to eventually yield $WS_{2(1-x)}P_{2x}$. Figure 1b displays the scanning electron microscopic (SEM) image of the synthesized nanomaterial. The morphology resembles more to NR than to NW. Up on simultaneous phosphidation and sulfidation, the neighboring NWs perhaps fused into one another and/or interconnected with each other to account for the observed morphology tuning, which is similar with other reported work.[33] The change in morphology is more obvious from transmission electron microscopic (TEM) image in Figure 1c, which reveals the formation of NR with geometrically increased exposure of active sites. We tried keeping only S powder as precursor and obtained WS_2 nanotube (Figure S3, Supporting Information), which is quite expected and also has already been reported.[19] What is important here is the fact that simultaneous operation plays a crucial role in tuning the morphology of the final product to NR via interconnecting the adjacent NWs. Moreover, the high resolution transmission electron microscopy (HRTEM) image (Figure 1d) clearly indicates that the interlayer spacing of the as-synthesized NR is 0.62 nm equaling the d-spacing of hexagonal WS_2. As can be seen from the elemental mapping in Figure 1e, the three components (W, S, and P) making up the obtained material are distributed uniformly in the NR. The S:P ratio in $WS_{2(1-x)}P_{2x}$ is quantified to be 1:0.03 from energy dispersive x-ray (EDX) spectroscopic elemental analysis depicted in **Figure 2**a. Such small amount of dopant is not capable of bringing observable effect on the crystalline nature of pristine WS_2. Thus, X-ray diffraction (XRD) pattern (Figure 2b) of $WS_{2(1-x)}P_{2x}$ is almost similar to that of the undoped WS_2, whose major patterns are indexed to hexagonal phase (pdf#08-0237). The featured peaks are retained revealing the fact that the crystal structure is not evidently changed. However, the intensities of the peaks somehow reduced after P doping following the slight alteration of the crystal lattice, possibly interfering with the crystallization. The same result was reported for the case of P doped into carbon nitride.[34,35] The peak at 2θ value of about 25° is ascribed to the carbon characteristics peak emanating from the carbon fiber substrate.[36,37] Corroboration of the lattice spacing imaged in the HRTEM can be ascertained here to correspond to the (002) plane at 2θ value of 14.32. It is noteworthy that there is no obvious diffractogram corresponding to WP_x type components, evidencing the phase purity of our novel material. Characterization with respect to Raman spectroscopy (Figure 2c) was made to further confirm the formation of desired material. The peaks at around 322, 353, and 421 cm^{-1} are due to 2LA, E^1_{2g} (in-plane), and A_{1g} (out of plane) modes of vibrations in WS_2. Due to the possible changes in bond polarization, $WS_{2(1-x)}P_{2x}$ shows slight shifts in the position of Raman peaks. The same observation was made by Ouyang et al. for P doped CoS2[29] and Wand et al. for Mo doped WS_2.[38] In order to gain further insight into the surface chemical states of the constituents in$WS_{2(1-x)}P_{2x,}$ X-ray photoelectron spectroscopic (XPS) analysis was made. As shown in Figure 2d–f, W4f state can be identified at 33.18 eV

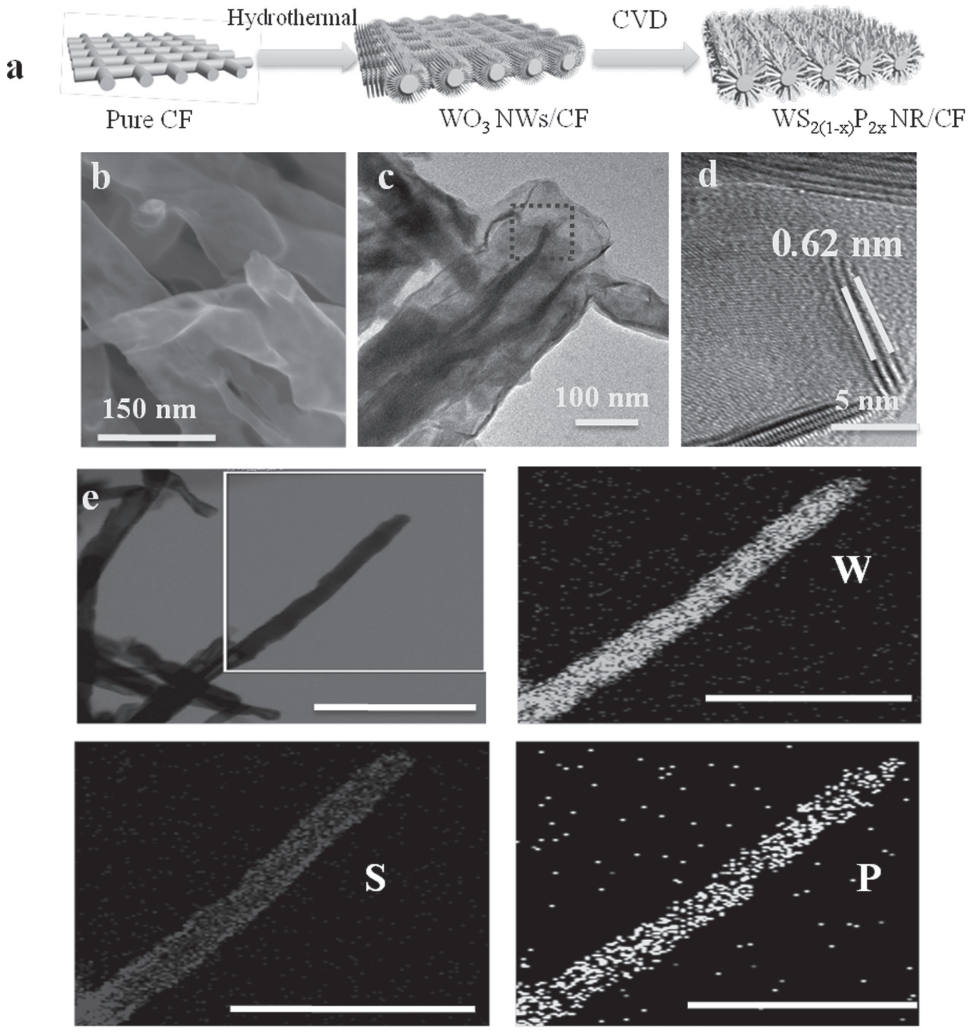

Figure 1. a) Schematic depicting the process of $WS_{2(1-x)}P_{2x}$ formation. b) SEM image, c) TEM image, and d) HRTEM image of $WS_{2(1-x)}P_{2x}$ NR. e) scanning transmission electron microscopy (STEM)–EDX elemental mapping evidencing the uniform distribution of W, S, and P in the entire matrix. The scale bars are 250 nm.

($W4f_{7/2}$) and 35.31 eV (W $4f_{5/2}$) and that of S 2p state at 162.8 eV (S $2p_{3/2}$) and 163.95 eV (S $2p_{1/2}$) for pristine WS_2. The profile of 2P region shows peaks at binding energies of 129.8 eV, which can be assigned to P $2p_{3/2}$ (P bonded to W), and 134.7 eV meant for superficial air oxidation (surface P-Ox) in $WS_{2(1-x)}P_{2x}$.[39,40] Shifts in the binding energies of XPS data are sources of valuable information.[41,42] Here, the peaks corresponding to W4f and S 2p regions shifted to lower binding energy in $WS_{2(1-x)}P_{2x}$ as compared to those in WS_2, evidencing the perturbation of electronic environment after incorporating smaller P anion with different electro negativity.

The electrocatalytic performances of the synthesized materials were then measured using a typical three electrode system in 0.5 M H_2SO_4 aqueous solution, wherein graphite rod served as counter electrode, saturated calomel electrode (SCE) as reference electrode, and our new material as working electrode (See the Experimental Section for details). Linear sweep voltammetric (LSV) test with *iR* correction (**Figure 3**a) was performed for the samples in order to extract information about their catalytic activity toward HER. The potentials were referenced to the RHE. For the sake of comparison, LSV tests of bare CF and benchmark catalyst, Pt, were made. The featureless polarization curve of CF guarantees the negligible HER activity. This brings a conclusive fact that the observed catalytic activity for other samples on CF solely emanates from the grown material. It is worth emphasizing that phosphorous doping into WS_2 markedly enhanced the HER catalytic activity as can be noticed from the recorded small overpotential of –98 mV (vs RHE) to achieve a current density of –10 mA cm^{-2} for $WS_{2(1-x)}P_{2x}$, as compared to –145 mV (vs RHE) for that of pure WS_2. The Tafel slope, derived from the polarization curve, is illustrated in Figure 3b for the sake of assessing the charge transfer kinetics in the process of catalyzing HER. As depicted, the $WS_{2(1-x)}P_{2x}$ NR possesses lower Tafel slope (71 mV per decade) as compared to the binary WS_2 nanotube (83 mV per decade), further reflecting the enhanced catalytic activity of the doped material via conveying a faster charge transfer kinetics. In order to evaluate more tangibly, we made cyclic

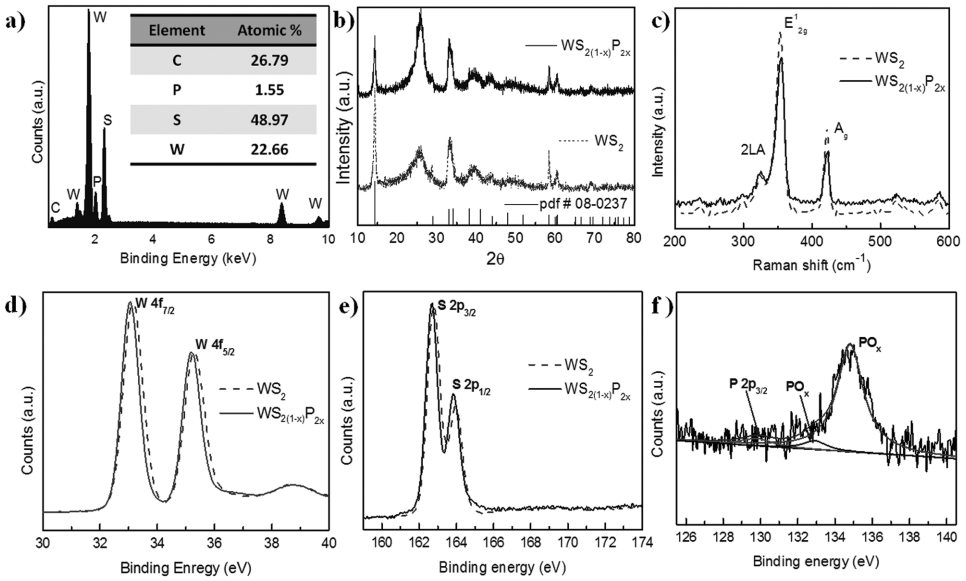

Figure 2. a) EDX spectra of $WS_{2(1-x)}P_{2x}$. XRD diffractogram along with the b) standard pattern, c) Raman spectra, of $WS_{2(1-x)}P_{2x}$ and WS_2. XPS spectra of d) W 4f region, e) S 2p region in $WS_{2(1-x)}P_{2x}$ and WS_2; and f) P 2p region in $WS_{2(1-x)}P_{2x}$.

voltammetry (CV) run at various scan rates (Figure S5, Supporting Information) to evaluate the double layer capacitance (C_{dl}) as an indication of electrochemical active surface area. As can be seen in Figure 3c, the C_{dl} value of $WS_{2(1-x)}P_{2x}$ NR (6.12 mF cm^{-2}) is considerably larger than that of WS_2 nanotube (0.91 mF cm^{-2}). It is to be noted that our procedure for synthesizing the desired material brought the advent of not only electronic perturbation, but also the change in morphology thereby accounting for the increased electrochemical surface area, which is consistent with the above characterizations. Moreover, the electrochemical impedance spectroscopic (EIS) characterization was conducted for further insight into the improved activity of the doped NR. Figure 3d illustrates Nyquist plot at 0.1 V (vs RHE) and the inset depicts the equivalent circuit model comprising three elements, i.e., solution resistance (R_s), constant phase element, and charge transfer resistance (R_{ct}). Accordingly, the R_s and R_{ct} values for $WS_{2(1-x)}P_{2x}$ NR are calculated to be 1.52 and 2.78 Ω, respectively, whereas for that of WS_2 nanotube are 2.4 and 25.72 Ω, respectively. Here, information about the reaction kinetics of the electrode can be traced on the basis of resistance values. For instance, the doped NR has faster electron transfer as compared to the pristine nanotube due to the smaller resistance values (smaller diameter of the semicircle in Nyquist plot).

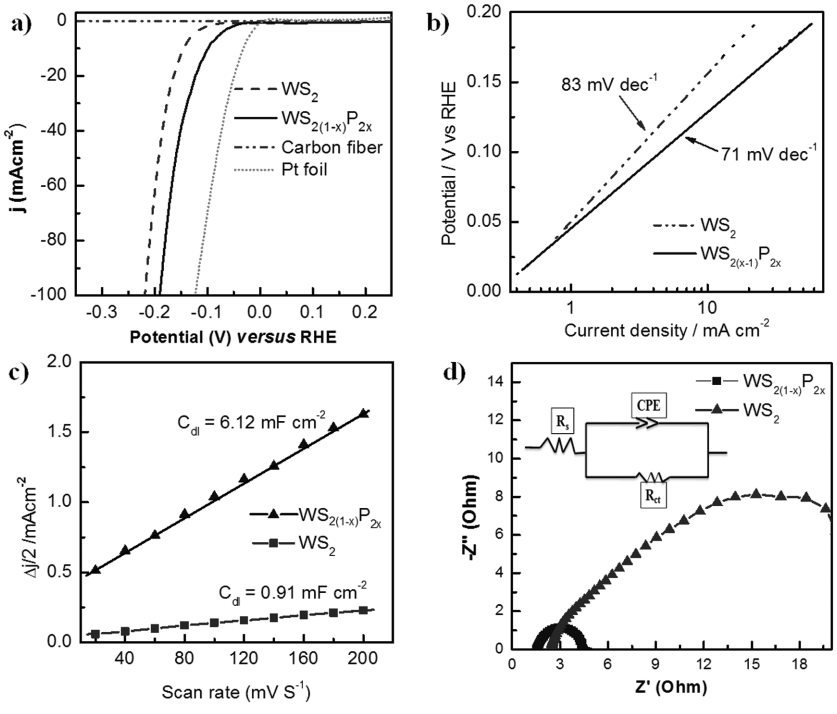

Figure 3. Electrochemical characterizations illustrating a) Polarization curves, b) Tafel plots, c) C_{dl} estimation for assessment of electrochemical active surface area, and d) EIS-Nyquist plot.

Apart from the very good catalytic activity, stability and durability are other key factors to evaluate the performance of a given electrocatalyst. In our experiment, the electrode under investigation, $WS_{2(1-x)}P_{2x}$ NR, was subjected to accelerated degradation test of 1000 continues CV runs at a scan rate of 100 mV s^{-1} to assess the stability. The polarization curve was obtained after such harsh test and compared with the one before the test. **Figure 4**a shows minor deterioration of catalytic performance after 1000 continuous CV cycles, suggesting its good stability. Furthermore, chronoamperometric

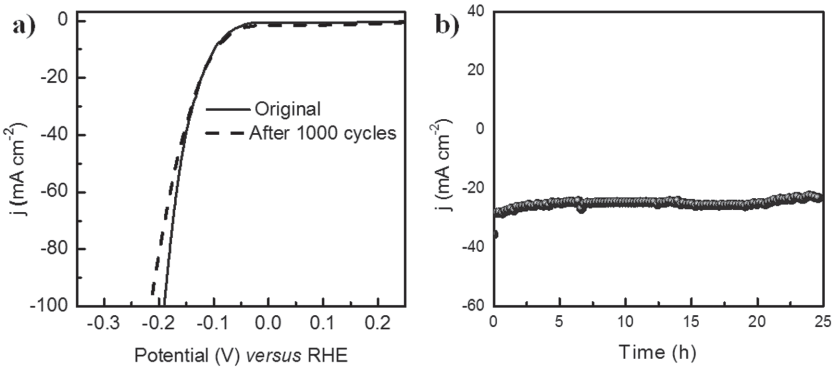

Figure 4. Stability and durability test results of $WS_{2(1-x)}P_{2x}$ NR for catalyzing HER. a) Polarization curves obtained before and after 1000 cycles of CV run for accelerated degradation test depicting negligible difference between the two. b) Chrono-amperometric *J–t* plot for durability test made at –0.15 V versus RHE.

J–t test at –0.15 V (vs RHE) was performed to evaluate the durability of the electrocatalyst. Continuous (for up to 25 h) generation of H_2 without any decay can be noticed from Figure 4b further solidifying the robustness of the catalyst.

3. Conclusion

In summary, we report a stepwise synthesis of $WS_{2(1-x)}P_{2x}$ NR via hydrothermal method followed by CVD method on flexible CF substrate for efficient catalysis of HER. The simultaneous phosphidation and sulfidation of WO_3 NWs resulted in the formation of $WS_{2(1-x)}P_{2x}$ NR, a morphology wherein the geometrical exposure of active site is more pronounced. Phosphorous doping merely affects the electronic environment in pristine WS_2 without causing considerable effect in the crystalline structure. The obtained material exhibited markedly enhanced HER performance. Being the first to attempt the incorporation of P into the lattice of WS_2 without affecting the crystalline structure, this approach can be a platform to design and explore more using other TMDs.

4. Experimental Section

Synthesis of WO_3 NWs on CF: Hydrothermal method was followed to synthesize WO_3 NWs on CF. Prior to the growth, a piece of CF was cut and ultrasonically cleaned with acetone, ethanol, and water. In a typical synthesis, 4.11 g of sodium tungstate dihydrate ($Na_2WO_4{\cdot}2H_2O$) and 3.15 g of oxalic acid ($H_2C_2O_4$) were dissolved in deionized water, through dropwise addition of water till clear solution appears. Subsequently, 313 µL of conc. HNO_3 was added in the above solution under vigorous stirring. This solution was diluted to 250 mL, from which 50 mL was transferred to Teflon-lined stainless autoclave containing 2 g of $(NH_4)_2SO_4$. After complete dissolution, the cleaned CF was put into the autoclave. The content was then sealed and further protected by iron cover for hydrothermal treatment at 180 °C for 16 h. After the hydrothermal reaction, the CF was taken out, rinsed with deionized water repeatedly, and dried at 60 °C in an ambient air. The CF, onto which growth took place, was then annealed in air at 500 °C to reduce oxygen defects in the desired WO_3NW.

Synthesis of $WS_{2(1-x)}P_{2x}$ NR on CF: A two-zone CVD furnace was used to synthesize $WS_{2(1-x)}P_{2x}$ NR via simultaneous sulfurization and phosphorization. Two inner tubes of different diameter (narrower and wider) were used in our CVD operation for concentrating the vapor at the deposition zone. The length of the tubes is equivalent to the distance from the front zone to back zone; hence, their ends coincide with the thermal centers in the respective zones (Figure S2, Supporting Information). Briefly, 0.1 g of red phosphorous powder was first mixed with 0.3 g of sulfur powder using mortar and pestle. The amount of P and S was varied so as to get optimum P dopant into WS_2, which was accomplished via measuring the HER performances for each (Figure S4, Supporting Information).The mixture of the powders was then kept at the bottom of the narrower tube, and the above synthesized WO_3 NWs/CF was kept at the other end. After that, the narrow tube was inserted into the wider tube such that the opening of one faces toward the bottom of the other. This setup was then placed in a CVD furnace chamber keeping the mixture of powders side in the front zone, while WO_3 NWs/CF side in the back zone. Then, the system was flushed with Ar gas for three times and pumped down to vacuum lower than 1 Pa. The temperature of the front zone was set to increase to 280 °C at a rate of 8 °C min^{-1} and that of the back zone to 800 °C at a rate of 26 °C min^{-1}. With such setting, the furnace was made to run for 1 h under 100 sccm Ar gas flow. Eventually, the furnace was allowed to cool down to room temperature, the product was used as electrocatalyst without any further treatment.

Material Characterization: The morphology and crystal structure of the sample were investigated through field emission scanning electron microscopy (Hitachi S4800 FESEM) and transmission electron microscopy (FEI Tecnai F20 TEM). XRD (D/MAX-TTRIII (CBO) diffractometer) was used to acquire X-ray diffractograms using Cu Kα radiation. Elemental mapping images were obtained from STEM–EDX equipped on TEM-2100F (200 kV). Information about Raman spectra was gathered from confocal microscope-based Raman spectrometer (Renishaw InVia) in ambient air environment with an excitation laser line of 532 nm. ESCALAB 250 Xi (system of Thermo Scientific) was employed to get the XPS spectra. The analysis chamber was 1.5×10^{-9} Mbar and the X-ray spot was 500 µm.

Electrochemical Measurements: Electrochemical characterization was performed with a typical three electrode system using CHI 660D potentiostat (CH Instruments, China). The setup consists of a counter electrode (graphite rod), reference electrode (SCE), and working electrode (the electrocatalyst under investigation). All the experiments were conducted in 99.99% N_2-saturated 0.5 M H_2SO_4 aqueous solution and the recorded potentials were referenced to a RHE. LSV was performed at a scan rate of 5 mV s^{-1} to test the HER performance of the electrocatalysts. The potentials in electrochemical characterizations were corrected for *iR* losses except for the study of C_{dl} estimation and durability test. Electrochemical impedance spectroscopic measurements were conducted at an applied voltage of 0.1 V versus RHE in a frequency range of

0.01 Hz to 0.5 MHz. The determination of double layer capacitance was performed by running various cycles of cyclic voltammetry differing only in scan rates (20–200 mV s^{-1}) in the potential range of 0.1–0.2 V, versus RHE.

Supporting Information

Supporting Information is available from the Wiley Online Library or from the author.

Acknowledgements

This work was supported by Ministry of Science and Technology of China (Grant No. 2016YFA0200700), National Natural Science Foundation of China (Grant Nos. 21373065, 61474033, 61574050, and 11674072), Strategic Priority Research Program of the Chinese Academy of Sciences (Grant No. XDA09040201), and CAS Key Laboratory of Nanosystem and Hierarchical Fabrication. The authors also gratefully acknowledge the support of Youth Innovation Promotion Association, CAS and CAS-TWAS president's fellowship.

[1] D. Larcher, J. M. Tarascon, *Nat. Chem.* **2015**, *7*, 19.
[2] P. Rogers, *Environ. Sci. Technol.* **1991**, *25*, 580.
[3] J. R. Rostrup-Nielsen, *Catal. Rev.* **2004**, *46*, 247.
[4] J. A. Turner, *Science* **2004**, *305*, 972.
[5] G. W. Crabtree, M. S. Dresselhaus, M. V. Buchanan, *Phys. Today* **2004**, *57*, 39.
[6] J. Greeley, T. F. Jaramillo, J. Bonde, I. B. Chorkendorff, J. K. Norskov, *Nat. Mater.* **2006**, *5*, 909.
[7] Y. Zheng, Y. Jiao, M. Jaroniec, S. Z. Qiao, *Angew. Chem., Int. Ed.* **2015**, *54*, 52.
[8] D. Voiry, J. Yang, M. Chhowalla, *Adv. Mater.* **2016**, *28*, 6197.
[9] W. F. Chen, J. T. Muckerman, E. Fujita, *Chem. Commun.* **2013**, *49*, 8896.
[10] F. Wang, T. A. Shifa, X. Zhan, Y. Huang, K. Liu, Z. Cheng, C. Jiang, J. He, *Nanoscale* **2015**, *7*, 19764.
[11] Y. Shi, B. Zhang, *Chem. Soc. Rev.* **2016**, *45*, 1529.
[12] J. Bonde, P. G. Moses, T. F. Jaramillo, J. K. Norskov, I. Chorkendorff, *Faraday Discuss.* **2009**, *140*, 219.
[13] T. F. Jaramillo, K. P. Jørgensen, J. Bonde, J. H. Nielsen, S. Horch, I. Chorkendorff, *Science* **2007**, *317*, 100.
[14] C. Tsai, K. Chan, F. Abild-Pedersen, J. K. Norskov, *Phys. Chem. Chem. Phys.* **2014**, *16*, 13156.
[15] J. Lin, Z. Peng, G. Wang, D. Zakhidov, E. Larios, M. J. Yacaman, J. M. Tour, *Adv. Energy Mater.* **2014**, *4*, 1301875.
[16] M. A. Lukowski, A. S. Daniel, C. R. English, F. Meng, A. Forticaux, R. J. Hamers, S. Jin, *Energy Environ. Sci.* **2014**, *7*, 2608.
[17] X. Zhao, X. Ma, J. Sun, D. Li, X. Yang, *ACS Nano* **2016**, *10*, 2159.
[18] Q. Gong, L. Cheng, C. Liu, M. Zhang, Q. Feng, H. Ye, M. Zeng, L. Xie, Z. Liu, Y. Li, *ACS Catal.* **2015**, *5*, 2213.
[19] K. Xu, F. Wang, Z. Wang, X. Zhan, Q. Wang, Z. Cheng, M. Safdar, J. He, *ACS Nano* **2014**, *8*, 8468.
[20] F. Wang, J. Li, F. Wang, T. A. Shifa, Z. Cheng, Z. Wang, K. Xu, X. Zhan, Q. Wang, Y. Huang, C. Jiang, J. He, *Adv. Funct. Mater.* **2015**, *25*, 6077.
[21] L. Yang, Q. Fu, W. Wang, J. Huang, J. Huang, J. Zhang, B. Xiang, *Nanoscale* **2015**, *7*, 10490.
[22] H. Li, Q. Zhang, X. Duan, X. Wu, X. Fan, X. Zhu, X. Zhuang, W. Hu, H. Zhou, A. Pan, X. Duan, *J. Am. Chem. Soc.* **2015**, *137*, 5284.
[23] J. Yu, Q. Li, Y. Li, C.-Y. Xu, L. Zhen, V. P. Dravid, J. Wu, *Adv. Funct. Mater.* **2016**, *26*, 7644.
[24] R. Ye, P. del Angel-Vicente, Y. Liu, M. J. Arellano-Jimenez, Z. Peng, T. Wang, Y. Li, B. I. Yakobson, S. H. Wei, M. J. Yacaman, J. M. Tour, *Adv. Mater.* **2016**, *28*, 1427.
[25] Q. Fu, L. Yang, W. Wang, A. Han, J. Huang, P. Du, Z. Fan, J. Zhang, B. Xiang, *Adv. Mater.* **2015**, *27*, 4732.
[26] X. Xie, R. Yu, N. Xue, A. B. Yousaf, H. Du, K. Liang, N. Jiang, A.-W. Xu, *J. Mater. Chem. A* **2016**, *4*, 1647.
[27] W. Liu, E. Hu, H. Jiang, Y. Xiang, Z. Weng, M. Li, Q. Fan, X. Yu, E. I. Altman, H. Wang, *Nat. Commun.* **2016**, *7*, 10771.
[28] M. Caban-Acevedo, M. L. Stone, J. R. Schmidt, J. G. Thomas, Q. Ding, H.-C. Chang, M.-L. Tsai, J.-H. He, S. Jin, *Nat. Mater.* **2015**, *14*, 1245.
[29] C. Ouyang, X. Wang, S. Wang, *Chem. Commun.* **2015**, *51*, 14160.
[30] K. Liu, F. Wang, K. Xu, T. A. Shifa, Z. Cheng, X. Zhan, J. He, *Nanoscale* **2016**, *8*, 4699.
[31] K. Wang, C. Zhou, D. Xi, Z. Shi, C. He, H. Xia, G. Liu, G. Qiao, *Nano Energy* **2015**, *18*, 1.
[32] Y. Domi, H. Usui, M. Shimizu, Y. Kakimoto, H. Sakaguchi, *ACS App. Mater. Interfaces* **2016**, *8*, 7125.
[33] X.-D. Wang, Y.-F. Xu, H.-S. Rao, W.-J. Xu, H.-Y. Chen, W.-X. Zhang, D.-B. Kuang, C.-Y. Su, *Energy Environ. Sci.* **2016**, *9*, 1468.
[34] B. Chai, J. Yan, C. Wang, Z. Ren, Y. Zhu, *App. Surf. Sci.* **2017**, *391*, 376.
[35] A. Kumar, P. Kumar, C. Joshi, M. Manchanda, R. Boukherroub, S. Jain, *Nanomaterials* **2016**, *6*, 59.
[36] S. Ōtani, *Carbon* **1965**, *3*, 31.
[37] S.-S. Tzeng, K.-H. Hung, T.-H. Ko, *Carbon* **2006**, *44*, 859.
[38] Z. Wang, P. Liu, Y. Ito, S. Ning, Y. Tan, T. Fujita, A. Hirata, M. Chen, *Sci. Rep.* **2016**, *6*, 21536.
[39] Z. Pu, Q. Liu, A. M. Asiri, X. Sun, *ACS Appl. Mater. Interfaces* **2014**, *6*, 21874.
[40] J. Tian, Q. Liu, A. M. Asiri, X. Sun, *J. Am. Chem. Soc.* **2014**, *136*, 7587.
[41] B. Gao, Y. Ma, Y. Cao, W. Yang, J. Yao, *J. Phys. Chem. B.* **2006**, *110*, 14391.
[42] A. Nossa, A. Cavaleiro, *J. Mater. Res.* **2004**, *19*, 2356.

Received: November 4, 2016
Revised: December 27, 2016
Published online: February 6, 2017

